AN ABSTRACT OF THE THESIS OF

Tyler Dewey for the degree of Master of Science in Industrial Engineering presented on September 5, 2001. Title: Intermetallic Microlamination for High-Temperature Microreactors

Redacted for privacy

Abstract approved: _____

Brian K. Paul

Chemical microreactors offer opportunities for portable power generation, on-site waste remediation and point-of-use chemical synthesis. Much of the existing development of microreactor devices involves silicon-based microfabrication techniques. It is recognized that new refractory materials are important to realizing high-temperature microreactors. Requirements of these materials include high-temperature resistance, chemical inertness and low-cost microfabrication. Advances in multilayer ceramics hold promise for the fabrication of microreactor structures from ceramic tape. Problems include creep, moderate levels of densification, and volumetric shrinkage, all of which can lead to dimensional instability.

Intermetallics are another class of refractory materials which may hold some promise for high-temperature microreactor development. In this paper, a new method of forming microchannel arrays from thin layers of intermetallics is demonstrated. This method has the advantage of eliminating volumetric shrinkage due to binder removal. Various iterations of NiAl intermetallic conversion and bonding are presented. Results

show that the NiAl system may be suitable as a substrate for microchannel reactor designs.

Intermetallic Microlamination for High-Temperature Microreactors

by

Tyler Dewey

A THESIS

submitted to

Oregon State University

In partial fulfillment of
the requirements for
the degree of

Master of Science

Presented September 5, 2001
Commencement June 2002

Master of Science thesis of Tyler Dewey presented on September 5, 2001

APPROVED:

Redacted for privacy

Major Professor, representing Industrial Engineering

Redacted for privacy

Chair of Department of Industrial and Manufacturing Engineering

Redacted for privacy

Dean of Graduate School

I understand that my thesis will become part of the permanent collection of Oregon State University libraries. My signature below authorizes the release of my thesis to any reader upon request.

Redacted for privacy

Tyler Dewey, Author

TABLE OF CONTENTS

LIST OF FIGURES

LIST OF FIGURES (continued)

LIST OF TABLES

1. INTRODUCTION

Microtechnology-based Energy and Chemical Systems (MECS) are microfluidic devices that rely on embedded microstructures for their function. The overall size of MECS devices places them in the mesoscopic regime, i.e. in a size range between macro objects such as automobile engines and laboratory vacuum pumps, and the intricate MEMS-based sensors that reside on a silicon chip. Thus MECS, although having micro features, are large by MEMS standards straddling the size range between the macro- and micro-worlds.

The internal processes of MECS devices rely on length scales that are much smaller than traditional systems. For thermal and chemical applications, small length scales provide the benefits of high rates of heat and mass transfer, large surface-to-volume ratios, and the opportunity to operate at elevated pressures. For other applications, small dimensions imply rapid response and compact design. Because of this, MECS devices are expected to provide a number of important functions whenever a premium is placed on either mobility, compactness, or point application. For example, the development of miniature refrigerators could provide point cooling of high speed electronics and communication equipment, enhancing performance.[1] Also, power packs based on combustion (rather than electrochemistry) could extend the operating times of electronic devices by a factor of ten.[2] In the area of chemical processing, miniaturized chemical reactors could provide on-site neutralization of toxic chemicals, thereby eliminating the need for transport to the remediation site, and/or burial.[3] Because many MECS devices

rely on fluidic processes, the same technology can be applied to biological applications. Miniaturized bioreactors could provide precisely regulated environments for small groups of cells to enhance their production of therapeutic drugs, or the detection of toxic compounds.

It is expected that these miniature devices can be produced in highly-parallel arrays at low cost, similar to Integrated Circuits and MEMS devices. IC and MEMS manufacturing rely heavily on silicon-based processing. In the IC industry, sub micron features are routinely implemented in production. However, MECS do not require the extremely small feature sizes needed to fabricate ICs. Furthermore, for many MECS applications, silicon is not the favored base material.[4 5] It has a much higher thermal conductivity than is desired for energy-based applications and the material, although strong, is brittle, expensive, and cannot always be tailored to specific environmental conditions. In contrast, the functionality of MECS typically require that they have the thermal, chemical, and physical properties of more traditional engineering materials such as metals or ceramics.

One subclass of MECS devices that is receiving a significant and growing amount of research interest is high-temperature micro reactors. Material requirements include high melting temperatures and good corrosion resistance. Examples of high-temperature micro reactors include a microchannel catalytic combustor/reactor and a gasoline vaporizer that have been produced at Pacific Northwest National Laboratories.[6 7] The material used in this application was type 316 stainless steel with channel widths on the order of 250 micrometers. The devices were tested up to a temperature of 650°C. Researchers in Germany created a microchannel heat exchanger that is used in a

miniaturized reactor for the synthesis of HCN.[8] The microchannels were fabricated in stainless steel and were on the order of 60 microns wide.

Because these devices were fabricated in stainless steel, the maximum operating temperature of these devices is in the range of 600°C. Operation above this temperature would cause device failure due to creep or other high temperature related phenomena. However, there exist numerous applications for microchannel devices at temperatures higher than this. For example, hydrogen steam reforming for hydrogen production typically operates in the region of 650 to 800°C. Further applications of current interest for high temperature heat exchangers include[9]:

- Steam superheating for driving turbines
- Gasification of coals and heavy oils
- Flue gas desulphurisation
- Chemical, petroleum, petrochemical and metallurgical process waste heat recovery and process heating
- Incineration, especially of hazardous materials
- Domestic furnace waste recovery
- Mobile engine heat recovery

Ceramics have been identified as a possible structural material for these devices because of their very high melting point, low thermal conductivity, and corrosion resistance. Some work has been conducted with the use of multi-layer ceramics to form microchannel conduits, but this work is still in its infancy.[10 11 12] These processes have developed microchannels 500μm wide with low aspect ratio geometries. When trying to create smaller geometries with higher aspect ratios, the problems with ceramics include

warpage due to shrinkage during binder removal, warpage due to sagging and low fractional densities.

Another group of materials with physical properties similar to those of ceramics are intermetallics. Intermetallics have good high-temperature properties, but, like ceramics, have poor formability at room temperature. Past research at the U.S. Department of Energy Albany Research Center has shown that various intermetallics can be synthesized from elemental foils through heat treatment.[13] Therefore, one alternative to forming intermetallics would be to form the ductile elemental foils at room temperature and afterwards synthesize the intermetallic foils simultaneously at high temperature. This paper will present current results toward forming intermetallic microchannels with this method.

2. METHODS

NiAl was chosen for this experiment because of its high temperature capabilities and good corrosion resistance. The binary phase diagram for NiAl is shown in Figure 1[14]. Further, Table 1 compares the yield strength, ultimate tensile strength, and % elongation for Ni and IC-218LZr (82.9% Ni, 8.5% Al, 7.8% Cr, 0.8% Zr, 0.02% B) at elevated temperatures.[14 15] Also, Figure 2 compares the yield stress of Ni_3Al to stainless steel at elevated temperatures[16]. Although the melting temperature of NiAl is not much higher than that of Ni and the melting temperature of Ni_3Al is in fact lower than Ni, the high temperature mechanical properties of nickel aluminides are much better. These diagrams illustrate the excellent high temperature properties of NiAl.

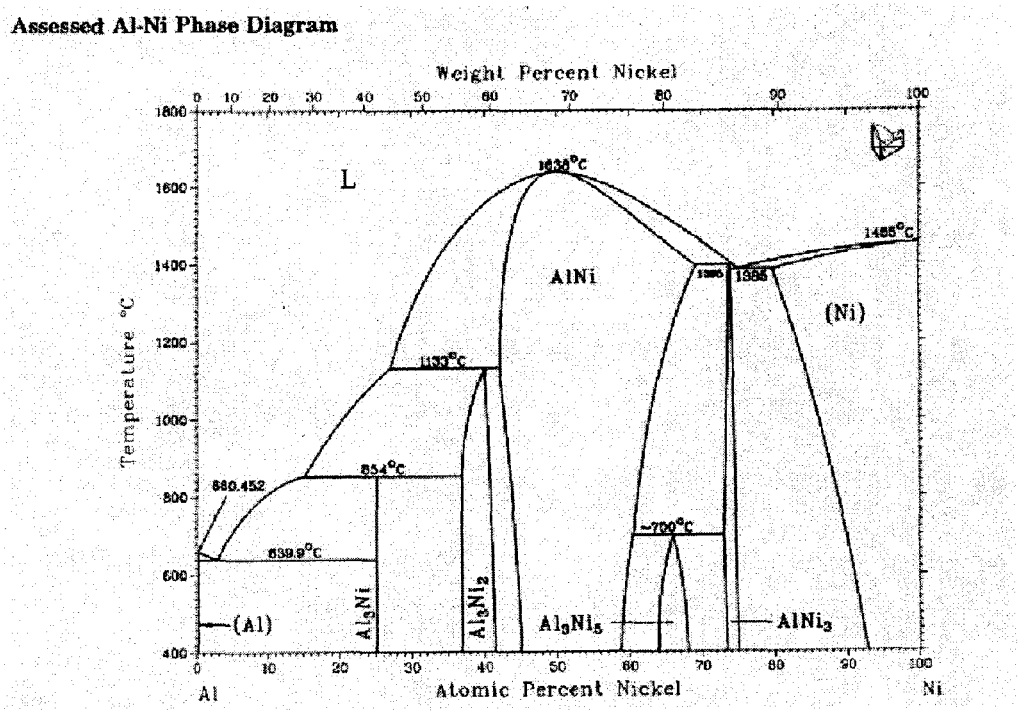

Figure 1 NiAl Phase Diagram

Table 1 Comparison of Ni and IC-218LZr (82.9% Ni, 8.5% Al, 7.8% Cr, 0.8% Zr, 0.02% B) Mechanical Properties at High Temperatures

	0.2% Yield Strength (MPa)		Ultimate Tensile Strength (MPa)		Total Elongation (%)	
Temp (°C)	Ni	IC-218LZr	Ni	IC-218LZr	Ni	IC-218LZr
600	110	602	250	689	60	11.7
800	N/A	529	170	676	60	7.5
1000	N/A	222	N/A	246	N/A	19.3

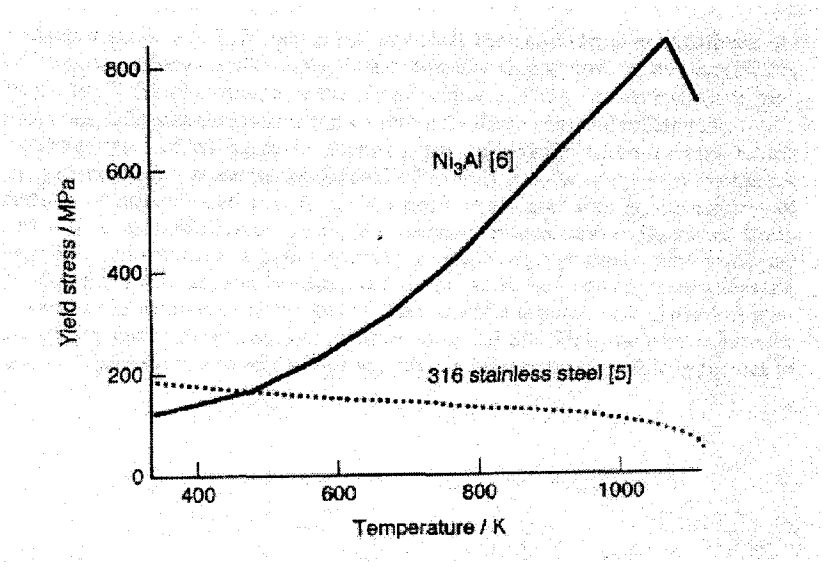

Figure 2 Graph of Yield Stress vs. Temperature for Ni_3Al

A microlamination procedure was used to form a NiAl intermetallic microchannel geometry. This procedure involved lamina patterning, laminae registration, and laminate bonding and conversion to intermetallic. Composite lamina blanks were produced by tack bonding of elemental foils within a vacuum hot press. Lamina patterning of the blanks was performed via laser ablation with a 532 nm Nd:YAG laser. A fixturing die was used to register the composite laminae before being tack bonded using an adhesive

material. Laminate bonding and conversion to intermetallic involved heat treating the tack-bonded stack of laminae in a vacuum furnace until the elemental foils reacted, resulting in a homogeneous intermetallic structure. Figure 3 summarizes these processing steps.

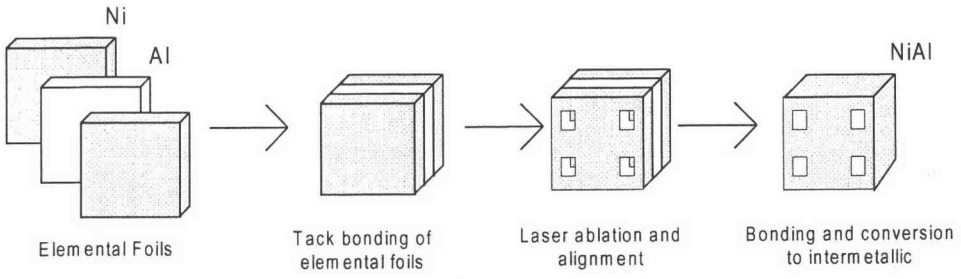

Figure 3 Illustration of microlamination procedure used

Figure 4a shows the actual laminae stack used to create the microchannel geometry. Figure 4b gives a picture of the fabricated microchannel array.

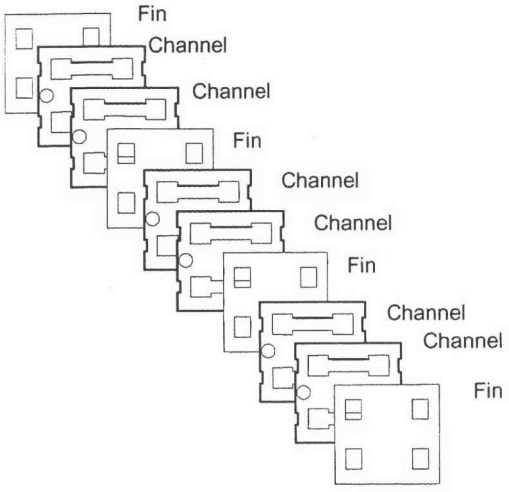

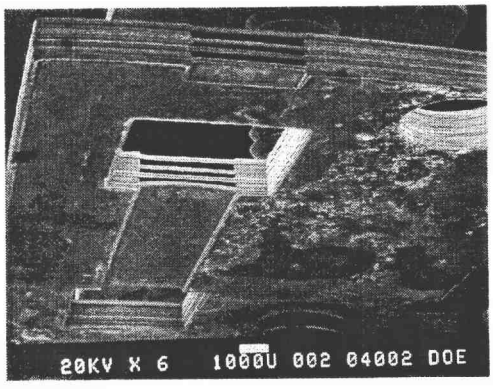

Figure 4a Laminae stack used

Figure 4b Microchannel array

The laminae were formed using 25.4 μm thick Al foil and 50.8 μm thick Ni foil. The foils were cut into 7.5 cm x 7.5 cm blanks. The blanks were cleaned using acetone, then acid-etched to remove native oxides. The Ni blanks were etched with a solution consisting of 20% by volume HCl and 80% by volume distilled water. The Al blanks were etched with a solution consisting of 50% by volume HNO_3 and 50% by volume distilled water. The blanks were agitated in solution for approximately five minutes. A composite blank consisting of one Ni blank sandwiched by two Al blanks was produced by low-temperature tack bonding in a vacuum hot press at 500°C and 1000 psi for 15 minutes. Once the composite blank was formed, an ESI 4420 Laser Micromachining System with a Q-switched 532 nm Nd:YAG laser rail was used to produce a patterned lamina from the blank.

Laminae registration was accomplished by using a fixture that used alignment pins corresponding to alignment holes cut into the laminae. This fixture is illustrated in Figure 5.

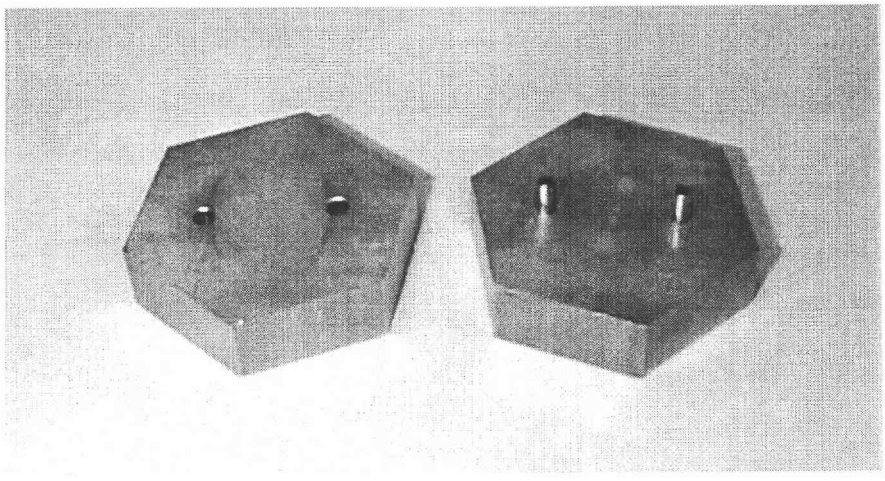

Figure 5 Fixture used for alignment of laminae

The laminae were adhesively bonded at room temperature and 700 psi. Poly Methyl Mathralate was used for adhesion. The final step was conversion of the laminae to an intermetallic compound by heat treating the adhesively bonded stack in a vacuum oven.

Experiments were initially conducted to determine the necessary cycle time in order to completely convert the samples to a homogeneous intermetallic compound. Figure 6 shows the intermetallic conversion progression through time. In Figure 6a three distinct phases are shown as indicated by the arrows. The middle phase is Ni, the outer phases are Al and the phases in between are nickel aluminides. In Figure 6b the aluminum and nickel phases have almost been extinguished. In Figure 6c, a homogeneous microstructure is shown. It was found that after 10 hours, the elemental foils had completely converted to intermetallic. Notice that the Al layers initially show porosity which has disappeared after full conversion. Notice also that the lamina thickness has decreased indicating a volumetric shrinkage due to the final density of the NiAl being greater than the average density of the elemental foils.

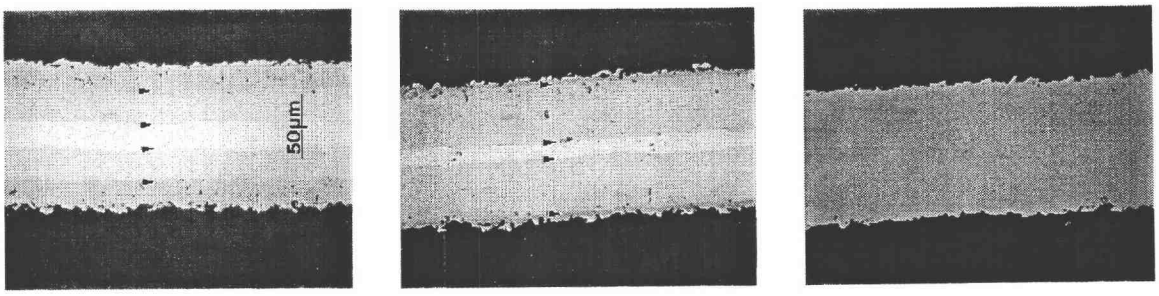

Figure 6 : Illustration of conversion of elemental Ni and Al to NiAl over time

a) 2 hours **b) 4 hours** **c) 10 hours**

The final sample was fixtured between two TZM platens with approximately 70 psi pressure and heated at a rate of 10°C per minute to a temperature of 1000°C. The sample was then held at this temperature for 10 hours to allow for the elemental foils to react to form NiAl. A description of the iterations necessary to develop this procedure are presented in Appendix B.

3. EXPERIMENTAL

3.1 Warpage

The functionality of MECS devices are greatly dependent on the ability to control microchannel dimensions. An experiment was performed to investigate the dimensional instability within the intermetallic microchannels. The two variables investigated in this experiment were the material used and laminae alignment. A 2 X 2 matrix was created using two levels for each variable. For the material NiAl and Ni were used to establish whether the conversion process contributed to dimensional instability. For laminae alignment, two levels were identified: good and poor alignment. Prior investigations had suggested that mis-alignment could be a significant factor contributing to fin warpage.[17] Good alignment was defined as the laminae alignment using the current fabrication procedure. Bad alignment was simulated by pattering two different microchannel geometries. The channel heights on each finished device were measured at three different points on the device end. The average and standard deviation were calculated for each channel. For a more detailed discussion of the experimental set-up, see Appendix C.

3.2 Volumetric Shrinkage

In order to better characterize the volumetric shrinkage, dimensional studies were performed. An ROI Optical Video Probe was used in conjunction with a Mitutoyo BHN coordinate measuring machine to take all measurements. Two sets of lateral measurements were taken. The first set of measurements were taken to compare the

change in lateral dimensions before and after intermetallic conversion. A measurement coupon was made by laser ablating a 5 X 5 mm square feature into a single composite lamina and converting it to intermetallic. A second set of measurements were taken to compare the change in lateral dimensions of a stack of laminae before and after conversion. This was done by laser ablating the same 5 X 5 mm feature into five laminae, which were then collectively bonded and converted.

Changes in laminae thickness were also monitored in this study. The thicknesses of samples were measured using a high-precision dial indicator. Measurements of laminae thickness are very important because this dimension determines the height of the microchannel. Three sets of thickness measurements were taken. The elemental foils were measured before being bonded as blanks. The composite Al-Ni-Al blanks were then measured after being tacked but before being cut. Finally, the thickness of various bonded intermetallic laminates consisting of bonded laminae were measured.

4. RESULTS

4.1 Warpage

The data collected in the warpage experiment was compiled and a statistical analysis was performed. Table 2 summarizes the data collected. An Analysis of Variance was completed for this data. ANOVA tables are presented in Appendix C.

Table 2: Summary of warpage experiment data

All dimensions in mm	**Ni**	**NiAl**	**Good Alignment**	**Poor Alignment**
Average channel height	0.1625	0.1650	0.1458	0.1817
Standard Deviation	0.0080	0.0295	0.0186	0.0189

This table shows that laminae alignment had the largest effect on average channel height. Referring the ratio of mean squares from Table 6 to the F distribution with 1 and 20 degrees of freedom shows that the probability that the ratio of mean squares is greater than 5.4 is 3.1% and that the ratio is greater than 5.9 is 2.5%. This data suggests a weak correlation between laminae alignment and mean channel height.

One interesting note, material did not have a significant affect on average channel height. It is believed this is because mean channel height may not be the best variable to use when investigating channel warpage. A device channel may have a large amount of warpage while the average height is very close to the expected value.

That is why a second variable was analyzed. The variance in channel height provides a better estimation of the warpage present throughout a channel. Therefore, the standard

deviation was calculated for the three points measured for each channel. Table 2 shows that the material used had the largest effect on channel height standard deviation. Referring the ratio of mean squares from Table 7 for material to the F distribution with 1 and 20 degrees of freedom shows that this value would be unusual if the null hypothesis that the standard deviation for the channel heights are equal was true. The probability that the ratio is greater than 10.4 is less than 1%.

This analysis suggests that the device material is a significant factor contributing to channel warpage. One explanation for the greater channel warpage using the NiAl

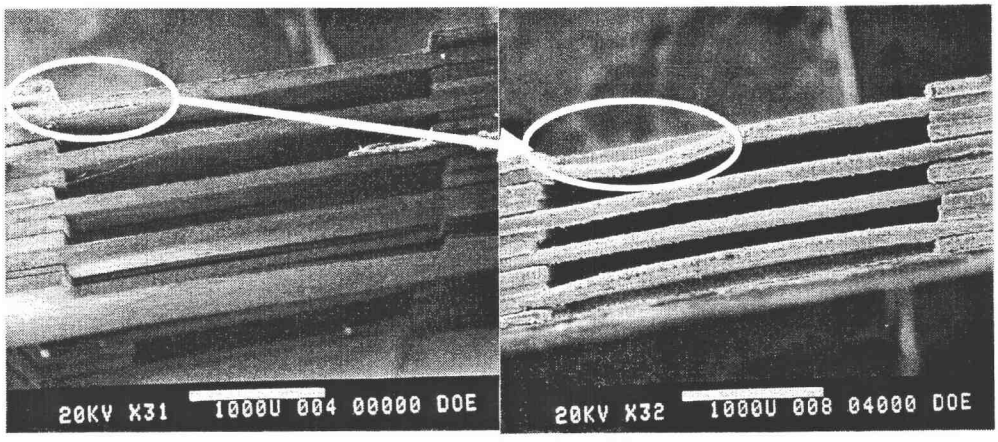

Before Heat Treatment **After Heat Treatment**

Figure 7 Illustration of delamination prior to intermetallic conversion contributing to fin warpage in the intermetallic sample

material is delamination of the composite Ni and Al foils before conversion to intermetallic. If this occurs then diffusion will not take place between the Ni and Al, and upon heating the conversion process will be only one-sided causing one side of the fin to shrink considerably in comparison to the high volume-to-mass aluminum foil. Figure 7 illustrates this phenomenon.

A cross section showing incomplete reaction of the elemental foils causing a non-homogeneous intermetallic material to form is shown in Figure 8a. Notice the deflection of the fin in the region in which the reaction is not complete. These events can cause extensive distortion of the fins above and below the channel during reactive bonding.

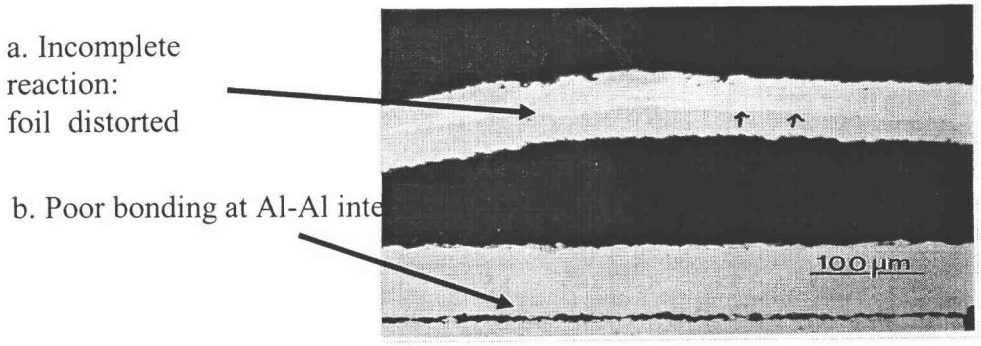

Figure 8 Cross Section of NiAl device showing a. deflected fin, b. poor bond between laminae at the Al-Al interface

4.2 Volumetric Shrinkage

The results of the lateral dimensional analysis are summarized in Table 3. Using these measurements the surface area for a fin was calculated. It was observed that the feature dimensions increased by less than 1% when a single lamina was converted to intermetallic. This was accounted for by the fact that NiAl has a slightly higher density than the elemental Ni and Al before conversion. Therefore, after conversion there is slightly less volume, causing the feature dimensions to be slightly larger. Because these are negative features being measured the larger dimension will correspond to less surface area and volume.

Table 3 Summary of lateral dimensional analysis

Description	Theoretical Dimension (mm)	Feature Width (mm)	Feature Height (mm)	Surface Area (mm^2)
Single lamina before conversion (Ni-Al)	5.000	5.007	5.009	502.60
Single lamina after conversion (NiAl)	5.000	5.056	5.052	500.75
Percent change		+0.98%	+0.86	-0.37%

The results of the laminae thickness investigation are summarized in Table 4. It was observed that the thickness decreased by as much as 17.3% after conversion to the intermetallic. This trend is consistent with the above dimensional analysis indicating that indeed the volume of material is decreasing due to a slightly higher density as a NiAl compound. Before and after conversion volumes for a fin were calculated using the data in Tables 3 and 4. It was found that there was 15.7% volumetric shrinkage. Although, NiAl's higher density only accounts for a volumetric change of 1.5%. It is theorized that the additional shrinkage can be accounted for by the fact that the outside dimensions of the laminate were not measured. Therefore the shrinkage that occurred in the vertical dimension may have actually been transferred to the overall outer dimensions of the laminate. The lateral features that were measured were somewhat constrained by being on the interior of the laminate, leading to very little change in the dimensions.

Table 4 Summary of thickness measurements

Description - # of laminae	Theoretical thickness μm	Actual thickness μm	Thickness per lamina (μm) [y]	Percent change [(y/x)-1]
Ni foil	50.8	50.9	50.9	-
Al foil	25.4	25.1	25.1	-
Ni-Al blank	101.6	99.3	99.3 [x]	-
single NiAl lamina	101.6	87.7	87.7	-11.7%
NiAl laminate – 3 stack	304.8	256.2	85.4	-14.0%
NiAl laminate – 5 stack	508.0	421.7	84.3	-15.1%
NiAl laminate – 9 stack	914.4	739.2	82.1	-17.3%
NiAl laminate – 13 stack	1320.8	1095.5	84.3	-15.1%

This analysis indicates that the bulk of the volumetric change will happen in the vertical dimension and that very little change in the interior lateral dimensions can be expected. As an example, see Figure 9. The width of the device channel before conversion was 3.00 mm. Measurement of this converted device gives a channel width of 2.977 mm validating the claim of minimal change of the lateral dimensions. This is an important result as the shrinkage in the vertical dimension can be expected to be much more uniform than the shrinkage in the lateral dimension which will be important for minimizing residual stresses.

4.3 Device

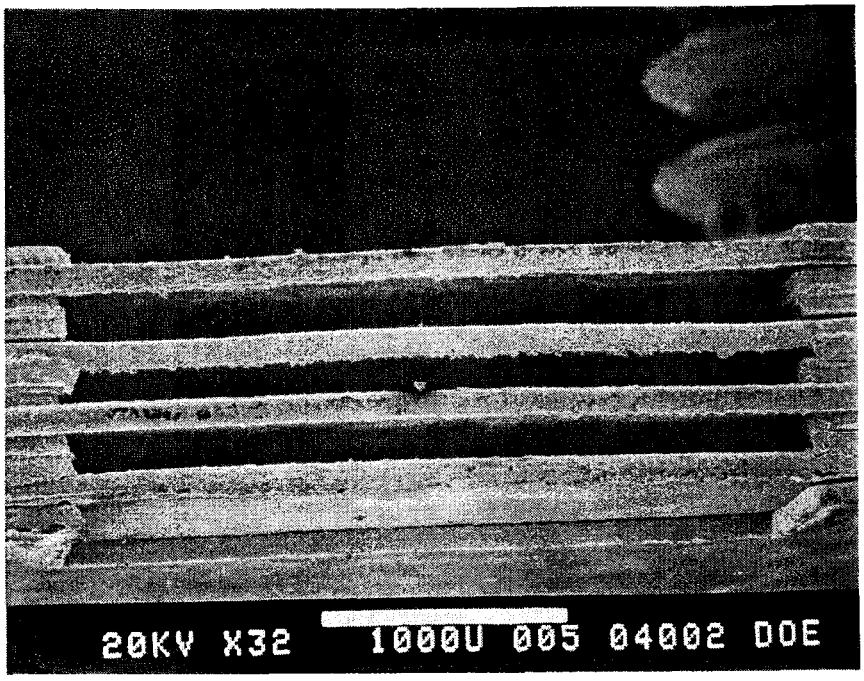

Figure 9 - Picture of NiAl microchannels created by microlamination and conversion of elemental Ni and Al foil.

Figure 9 shows a 32X picture of the microchannel array fabricated using the current design procedure. Channels are approximately 200 μm wide and fins are approximately 100 μm thick. One curious note is that though the reaction and heat treatment are carried out well in excess of the melting temperature of aluminum, the aluminum did not flow into the microchannels. Some experimentation showed that the aluminum did flow under modest bonding pressures. As a result, it is expected that the aluminum foil holds its shape because of the thick native oxides on its exterior which do not breakdown at the bonding temperature. Further, complete homogenization of the device was achieved after 10 hours of post reaction heat treatment indicating that the native oxides do not

sufficiently impede solid-state diffusion. It is surmised that a self-propagating, high-temperature reaction between the Ni and Al foil along the Ni-Al interface eliminates the diffusional barrier imposed by the native oxides.

Another interesting finding was the bond between laminae was very poor. This is again related to the thick native oxides of aluminum. This bond was forming at an Al-Al interface. It is theorized the oxides on each lamina combined with the low bonding pressure applied to the stack created a large barrier to diffusion. Figure 8b shows a cross section of a characteristic bond between laminae.

5. CONCLUSIONS

A microlamination procedure has been developed for fabricating microchannels as small as 200 μm wide and fins 100 μm thick within a monolithic NiAl intermetallic device. This method involves tack bonding a composite foil consisting of Ni and Al foils, precision machining the composite foil into laminae, sequentially stacking the laminae, and reactively synthesizing the composite foils along their interface followed by a post-synthesis heat treatment for diffusion bonding of laminae and stoichiometric homogenization.

A small, introductory, study to investigate the cause of channel deformation in the devices was also completed. As expected, it was found that the tendency for NiAl microchannels to have more warpage than plain Ni microchannels made by diffusion bonding was statistically significant. One explanation for this is delamination of the composite foils before conversion to an intermetallic.

Now that a satisfactory procedure has been developed for fabricating these devices, two opportunities for future research present themselves: (1) A more exhaustive study into the causes of channel deformation is needed. (2) A procedure in which the composite Ni and Al foils are less susceptible to damage during the pre-processing steps needs to be developed.

BIBLIOGRAPHY

[1] Little, W. A., "Microminiature Refrigerators for Joule-Thomson Cooling of Electronic Chips and Devices," *Advances in Cryogenic Engineering*, (Vol. 35,1990), pp. 1325-1333.

[2] Benson, R. S. and J.W. Ponton, , "Process Miniaturization- A Route To Total Environmental Acceptability?" *Trans. IChemE*, (Vol. 71, Part A, 1993), pp.160-168.

[3] Koeneman, P. B., I. J. Busch-Vishniac, and K. L. Wood, "Feasibility of Micro Power Supplies for MEMS," *J. MicroElectoMechanical Sys*, (Vol. 6(4), 1997), pp. 355-362.

[4] Peterson, R.B., , "Size Limits for Regenerative Heat Engines," *Microscale Thermophysical Engineering*, (Vol. 2, 1998), pp. 121-131.

[5] Peterson, R.B, "Numerical Modeling of Conduction Effects in Microscale Counterflow Heat Exchangers," *Microscale Thermophysical Engineering*, (Vol.3, 1999), pp. 17-30.

[6] Matson, D. W., P. Martin, D. Stewart, A. Tonkovich, M. White, J. Zilka, and G. Roberts, "Fabrication of Microchannel Chemical Reactors Using a Metal Lamination Process," *Proc. IMRET3,* (April, Frankfurt, Germany, 1999).

[7] Matson, D. W., P. Martin, A. Tonkovich, G. Roberts, "Fabrication of a stainless steel microchannel microcombustor using a lamination process", *Proc. Microchannel Devices and Components IV*, (Sept., Santa Clara, CA, 1998).

[8] Hessel V., W. Ehrfeld, K. Golbig, Ch. Hoffmann, H. Lowe, and M. Storz, "High temperature HCN gerneration in a complex integrated micro-reaction system," Proc. IMRET3, (April, Frankfurt, Germany, 1999).

[9] Chaumat, G. F. Moret, and A. Gasse, "SiC brazing for ceramic heat exchangers," DVS-Berichte, (v166, 1995), pp-217-219.

[10] Kim, M., Yi, M. Zhong, J., Bau, H.H., Hu, H. and Ananthasuresh, S.G.K., "The Fabrication of Flow Conduits in Ceramic Tapes and the Measurement of Fluid Flow through These Conduits," Proceedings of the ASME Dynamic Systems and Controls Division, DSC- (Vol. 66, 1998), pp. 171-177.

Bibliography (continued)

[11] Knitter, R, W. Bauer, B. Linner-Kremar, E. Hansjosten, "Rapid Manufacturing of Ceramic Microcomponents", Proc. EUROMAT 99, (Sept., Munchen, 1999)

[12] Knitter, R., D. Gohring, M. Bram, P. Mechnich, R. Broucek, "Ceramic Microreactor for High-Temperature Reactions," Proc. IMRET 4, (March, Atlanta, GA, 2000)

[13] Alman, D.E. and Dogan, C.P., "Intermetallic Sheets Synthesized from Elemental Ti, Al, and Nb Foils," Metallurgical and Materials Transactions A, (26A, October, 1995), pp. 2759-62.

[14] Brandes, E.A and Brook, G.B (Ed.), Smithells metal reference book, 1992, seventh edition

[15] Mirshams, A.R., R.H. Baldwin and V.K. Sikka, "High-temperature ductility of Intermetallic Nickel Aluminide IIC-218LZr," in High-Temperature Ordered Intermetallic Alloys IV, MRS Symposium Proceedings, LA Johnson et al. (Eds.), 1991, pp 649-654

[16]Golberb, D., Demura, M., Hirano, T., "Effect of Al-rich off-stoichiometry on the Yield Stress of binary Ni3Al single crystals", Acta Materiala, 1998, vol. 46, 99 2695-2703

[17] Paul, B.K., T. Dewey, D. Alman, R. Wilson,

[18] Sauthoff, G., Intermetallics, VCH Publishers, 1995

[19] Stoloff, N. S., V.K. Sikka, Physical Metallurgy and processing of Intermetallic Compounds, Chapman & Hall, 1996

[20] Anselmi-Tamburini, U., Z. A. Munir, "The propagation of a solid-state combustion wave in Ni-Al foils," *J. Appl. Phys.,* (Vol. 66 (10), 1989), pp. 5039-5045.

[21] Alman, D.E., C.P. Dogan, J.A. Hawk, J.C. Rawers, "Processing, structure and properties of metal-intermetallic layered composites", *Materials Science and Engineering*, (Vol. A 192/193 1995), pp. 624-632

Bibliography (continued)

[22] Alman, D.E, C.P. Dogan, "Intermetallic Sheets Synthesized from Elemental Ti, Al, and Nb Foils", *Metallurgical and Materials Transactions A,* (Vol. 26A, 1995), pp. 2759-2762

[23] V. Krause, H-g. Treusch, P. Loosen, T. Kimpel, J. Biesenbach, A. Kosters, F. Robert, H. Oestreicher, M. Marchiano, B. DeOdorico, "Microchannel coolers for high power laser diodes in copper technology", SPIE proceedings, (Vol 2148, 1995), pp. 351-358

[24] Walker, B., "Development of a Process for Fabricating High-Aspect-Ratio, Meso-Scale Geometries in Stainless Steel", *Master's Thesis*, Oregon State University, 1998

[25] Kazakov, N.F., Diffusion Bonding of Materials, Pergamon Press, 1985

[26] Terhaar, T., "Comparison of Two Microvalve Designs Fabricated in Mild Steel Using Microprojection Welding and Capacitive Dissociation", *Master's Thesis*, Oregon State University, 1998

APPENDICES

APPENDIX A: LITERATURE REVIEW

A.1 Intermetallics

A.1.1 General Information

One group of materials that have a unique set of properties is intermetallics. Intermetallics are a group of compounds which form as the result of the combination of various metals. According to one definition, intermetallics are compounds of metals whose crystal structures are different from those of the constituent metals.[18]

Intermetallics form because the bond strength between unlike constituent atoms is greater than the bond strength between like atoms. These compounds form crystal structures in which atoms are ordered and surrounded by unlike atoms. As a result of these crystal structures many intermetallic alloys possess properties desirable for high temperature applications, such as low thermal conductivity, low density, high melting temperature, and high corrosion resistance.[19] In recent years intermetallic compounds have become the focus of numerous studies because of these excellent high temperature properties.

A.1.2 NiAl

NiAl has been identified as an intermetallic with tremendous potential as a structural material because of its very high melting temperature, hardness, and chemical stability (corrosion resistance). NiAl crystallizes in the cubic B2 structure. This is a crystal structure with ordered atom distributions in which Ni atoms are surrounded by Al atoms. NiAl has a melting temperature of 1955 K, which is high even among intermetallics. NiAl also has a very large negative heat of formation, -72 kJ/mol, demonstrating its high

thermodynamic stability. Table 5 summarizes these and other physical properties of NiAl follows.[18]

Table 5 Physical Properties of NiAl

Property	NiAl
Bonding	Covalent/metallic
Melting point, K	1955
Density, g/cm^3	5.9
Young's Modulus, polycrystal, GPA	188
Shear modulus, polycrystal, GPA	71.5
Thermal expansion, 10^{-6}, 873 K	13.2
Specific Heat, J/g · K	.64
Thermal diffusivity, cm^2/sec	.22
Thermal conductivity, W/m · K	76

A.1.3 Intermetallic Synthesis

The process of forming intermetallic compounds by reacting elemental powders has been termed *self-propagating, high temperature synthesis* (SHS). Problems have occurred in modeling and predicting the behavior of these systems because of the complex nature of the reacting powders. A solution to this problem is a planar interface. It has been demonstrated that that a SHS reaction can be initiated at the interface of elemental foils.[20]

Intermetallic compounds have since been produced using a SHS reaction between elemental foils. Intermetallic laminar sheet composites have been produced based on the Ni-Al and Ti-Al systems.[21] These compounds were formed in a two step process: (a) a

reaction initiation sequence; (b) a post-reaction thermal aging step. It has been shown that a simple curved shape can be formed in an intermetallic compound by shaping the foils before initiating the SHS reaction.[13] This is a very promising result due to the fact that after conversion to an intermetallic it is very difficult and expensive to form these materials. This is due to the fact that the physical properties these materials possess are not conducive to either hot or cold deformation processing. More complicated ternary aluminides have also been produced directly from elemental foils.[21] It has been shown that a variety of intermetallic compounds can be produced through a SHS reaction between elemental foils and there exists potential for creating geometries with these compounds by pre-forming the foils.

A.2 Microlamination

Microlamination is a process in which high aspect ratio (large height to width ratio) geometries can be created in various substrates. The process consists of three steps, laminate formation, laminate registration, and laminate bonding. Formed laminates are stacked, aligned, and bonded together to form the desired geometry. Many geometries that cannot be created by other microfabrication process can be created using this method. One application currently being developed at Oregon State University (OSU) is a miniature alpha-Stirling cycle heat pump. This MECS device is being developed for use as a cryocooler for laser instrumentation. A MECS device of this type could theoretically increase the power of a typical laser diode by a factor of 2.3-3.1.[23] Researchers at OSU have used a new process called metal microlamination (MML) to create the high aspect ratio microchannels for this device.[24] This process has also been

used by researchers at PNNL to create a microchannel catalytic combustor/reactor and microchannel gasoline vaporizer.[6]

Laminate formation is the first step in microlamination. The laminates formed will provide the building blocks for the micro-device to be fabricated. The material being used and the dimensional requirements of the device are two factors used to decide laminate forming techniques. Chemical micromachining, photochemical etching, and laser ablation are three techniques commonly used for laminate formation. The devices created at PNNL used photochemical etching as the laminate formation technique, while the device created by Walker[24] used laser ablation.

Once the laminates are formed, they must be aligned with respect to each other, referred to as laminate registration. This can be done with features designed into the laminate or with external fixtures only. Examples of features designed into the laminates are alignment holes which receive alignment pins to hold the laminates in position, or notches in the laminate that correspond to geometries in an alignment fixture.

Once an alignment fixture has been designed the laminates must be bonded. The most common method used is diffusion bonding. This is a process for joining two materials which involves mating the surfaces of the materials, applying pressure, and then heating the materials. The materials are heated to a temperature at which one of the materials diffuses into another.[25] Other techniques for laminate bonding have also been used. Microvalves using the MML technology have been created using microprojection welding.[26]

APPENDIX B: DEVICE FABRICATION ITERATIONS

The first devices were created by tack bonding the laminae in a vacuum hot press for 15 min at 1000 psi before conversion to intermetallic. A 3-2-1 style graphite fixture was used to secure the laminae during this tacking step. Figure 10 shows the stack used in this iteration.

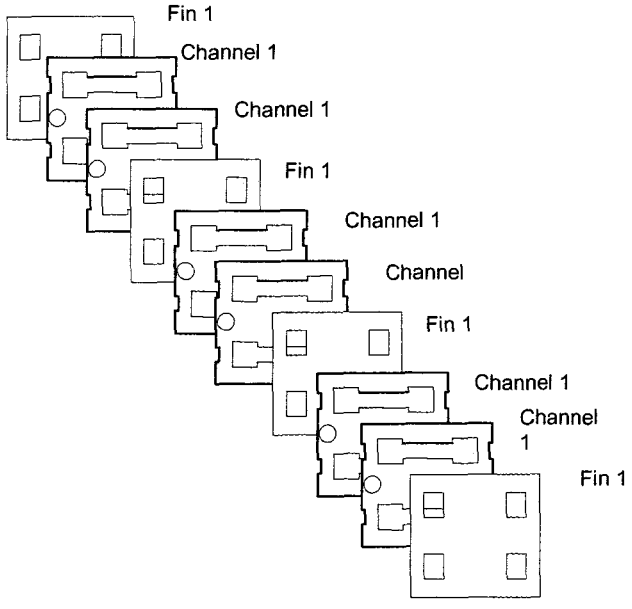

Figure 10 Laminae stack for first device fabrication attempt. (See Appendix D for detailed diagrams of laminae)

As shown in Figure 11, the first attempt at fabricating a device was unsuccessful due to severe warpage of the microchannel fins. The channels on this device have collapsed onto each other, possibly due to the severe misalignment of the laminae.

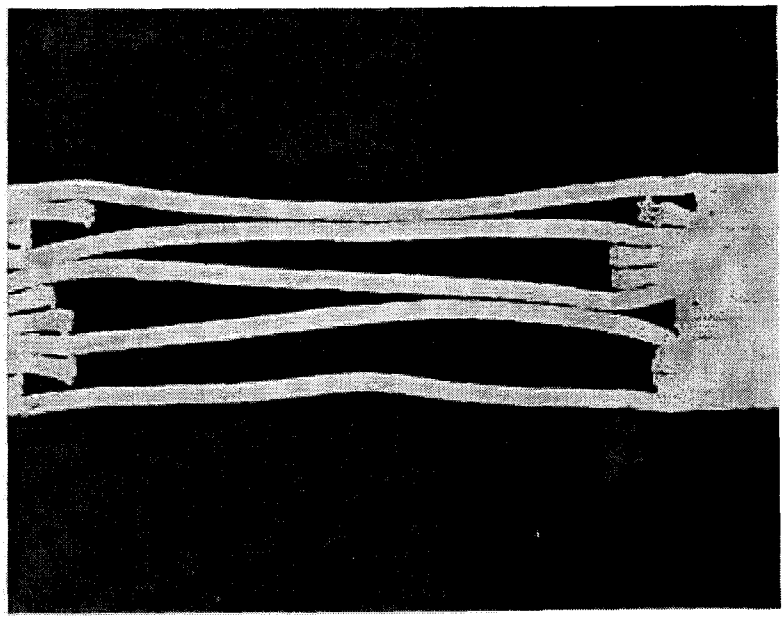

Figure 11 Micrographs of the first microchannel device, after conversion (50X)

In order to solve this problem, alignment notches were cut into the laminae to mate with the alignment pins on the graphite fixture used to tack bond the device. The stack use for this second device is shown in figure 12.

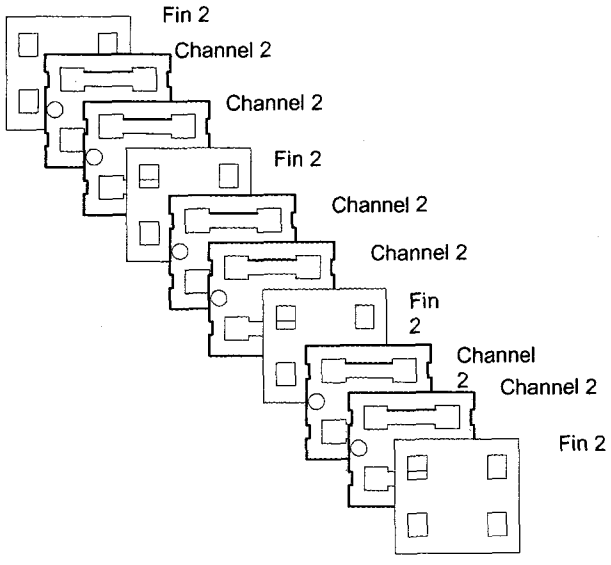

Figure 12 Laminae stack for second device fabrication attempt. (See Appendix D for detailed laminae diagrams)

The figure 14 shows a device fabricated using this alignment method. Figure 13a is the tack-bonded device not yet converted to NiAl. Figure 13b is the device bonded and converted to NiAl.

These pictures show that the alignment is improved, but the channels still exhibit a good deal of warpage. Figure 14a shows that a significant amount of warpage was

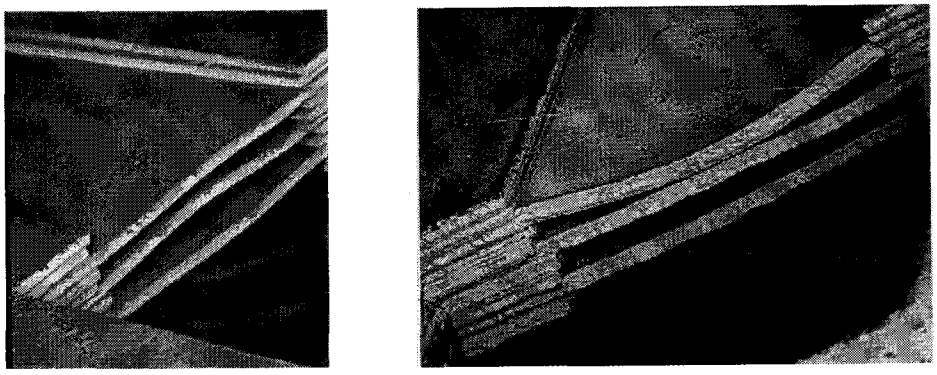

a) b)

Figure 13 Micrographs of the second microchannel device: a) after tacking and before conversion (26X) and b) after conversion (28X)

present before conversion to NiAl. Therefore, it was anticipated that the final warpage was not due solely to a creep-related phenomena since the tacking process was at moderate temperatures for short durations. Thus, the cause of this warpage was hypothesized to be a non-uniform tri-axial stress state caused by a mismatched coefficient of thermal expansion between the fixture and the laminate during tacking. The thermal expansion mismatch between the Al lamina and the graphite fixture was calculated to be 8.6 μm. Thermal expansion was not accounted for when creating this fixturing procedure and a transitional fit between the laminae and alignment pins was used. These two factors combined support the theory of a tri-axial stress being introduced due to CTE

mismatch. Further, the use of a transitional fit for registration may have led to the warpage of the composite laminae as shown in Figure 14a.

To validate this hypothesis, a third device was fabricated by eliminating thermal diffusion during the tack bonding step. Registration and tacking of laminae in the third device were accomplished by aligning the laminae in the alignment fixture and using an adhesive to tack them together. The laminae stack used is shown in Figure 4 (page 7) and the fixture is shown in Figure 5. The laminae were adhesively bonded at room temperature and 700 psi. Figure 14a below shows the device before conversion to NiAl. The figure shows that the warpage before conversion was dramatically reduced with this new procedure. Figure 14b shows that some warpage is still remaining within the microchannels. However, this is a large improvement compared with previous fabrication attempts.

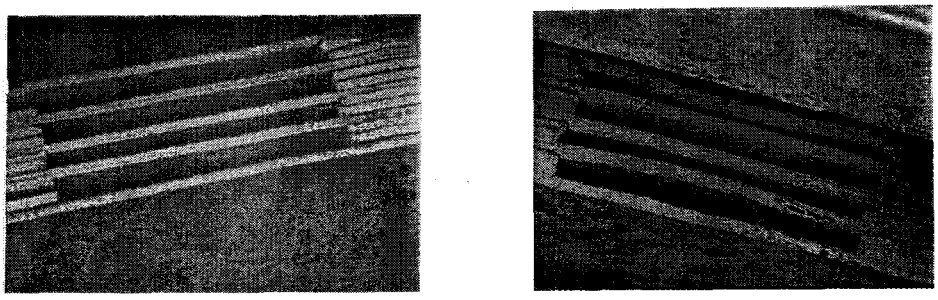

a) b)

Figure 14 - Micrographs of the third microchannel device a) after tacking and before conversion (24X) b) after conversion (27X)

APPENDIX C: SCREENING EXPERIMENT SET-UP

Once a suitable procedure for fabricating a microchannel device was developed a screening experiment was conducted to try to isolate the cause of channel warpage. Two variables were investigated in this experiment; material used (NiAl and Ni) and laminae alignment. The NiAl devices were fabricated as described in the Methods section of this paper. A composite NiAl blank was used to form the individual laminae. The Ni devices were created by using a 101.6 μm Ni blank instead of the composite NiAl blank. The same fabrication procedure was followed otherwise. Instead of a conversion to an intermetallic material, the Ni laminae simply diffusion bonded to each other.

The second variable investigated was alignment of the laminae. The two levels used were good and poor laminae alignment. Good alignment was considered to be the current procedure being used. Poor alignment was accomplished by forming laminae with altered dimensions to simulate misalignment. Figure 15 shows the laminae stack that was used to create the laminae with poor alignment.

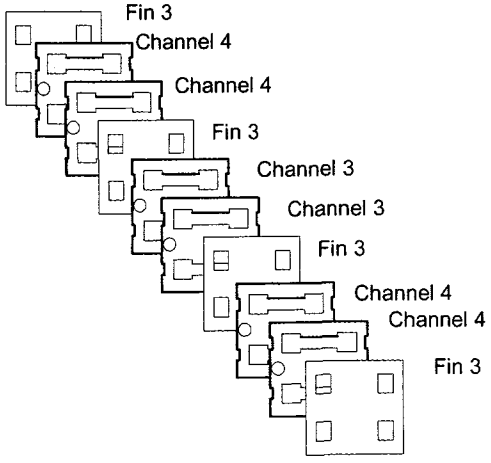

Figure 15 Laminae stack used to created devices with "poor" alignment. (See Appendix D for detailed laminae diagrams)

Once the devices were fabricated the height of each channel was measured at three evenly spaced points. This was accomplished by taking SEM pictures of the notches cut on the ends of the devices at a known magnification. These notches were used in order to obtain a picture that was perpendicular to the channel. (See Appendix D) Three parallel lines were drawn on tracing paper. This paper was placed on the pictures of the channels at a ninety degree angle. The channel height was measured at the three points the lines intersected the device fins. An example of the measurement taken is shown in Figure 16.

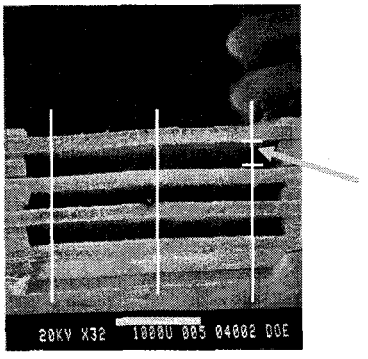

Each channel measured from fin to fin at three points

Figure 16 Measurement of device channel height

Data for the average height and standard deviation of each channel was collected and is shown in Appendix E. This data was used to create Analysis of Variance tables for the variables being investigated.

Table 6 ANOVA table for channel height average

Source	Sum of Squares X 10,000	DOF	Mean Square X 10,000	Ratio of mean squares, x	Probability Ratio > x
Alignment	77	1	77	5.4	0.031
Material	0	1	0	0	1
Interaction	84	1	84	5.9	0.024
Error	286	20	14.3		
Total	447	23			

Table 7 ANOVA table for channel height standard deviation

Source	Sum of Squares X 10,000	DOF	Mean Square X 10,000	Ratio of mean squares, x	Probability Ratio > x
Alignment	0	1	0	0	1
Material	28	1	28	10.4	0.004
Interaction	6	1	6	2.2	0.154
error	54	20	2.7		
Total	87	23			

APPENDIX D: LAMINAE DIAGRAMS (ALL DIMENSIONS IN MM)

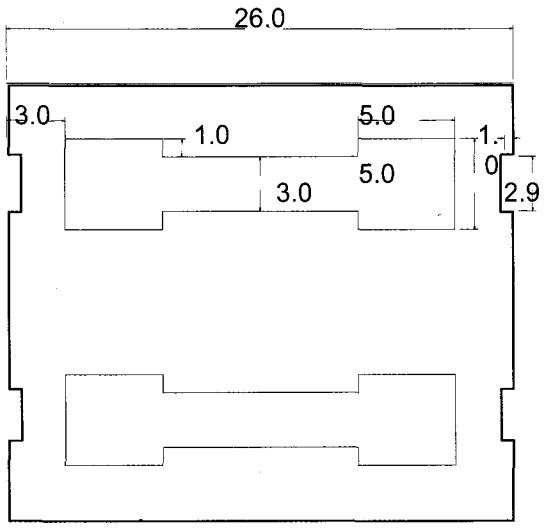

Figure 17: Channel 1 - Original design used. No alignment features used.

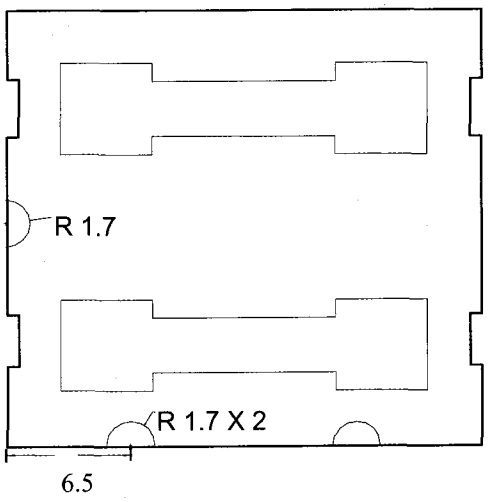

Figure 18: Channel 2 - Alignment notches cut into the side to match the alignment pins on the graphite fixture (dimensions the same as Figure 17 unless otherwise specified)

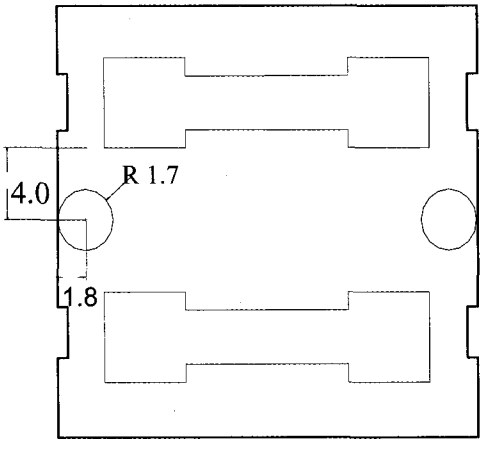

Figure 19: Channel 3 - Final design used. Alignment holes added to match with fixturing device (dimensions the same as Figure 17 unless otherwise specified)

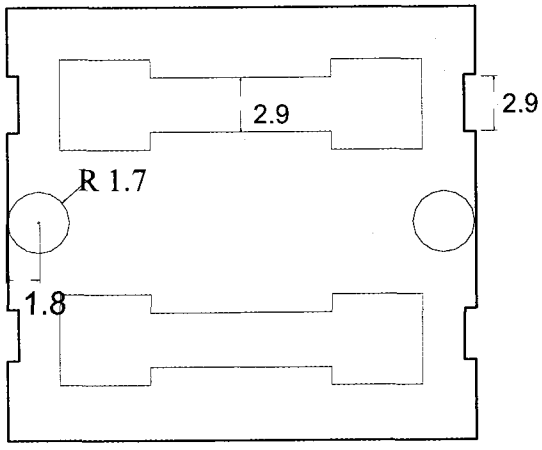

Figure 20: Channel 4 - Identical to channel 3 except channel width narrowed to simulate mis-alignment (dimensions the same as Figure 19 unless otherwise specified)

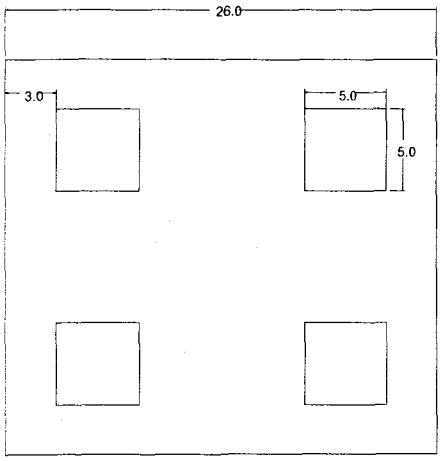

Figure 21: Fin 1 - Original design used. No alignment features used.

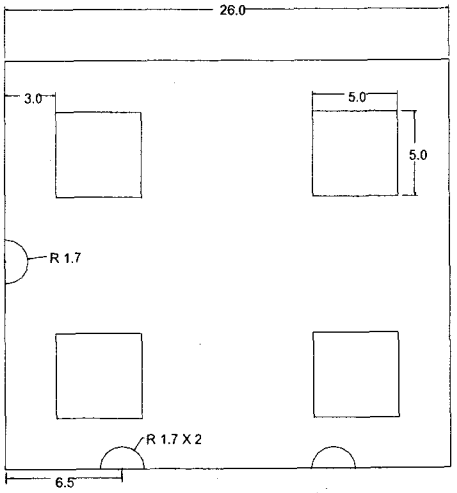

Figure 22: Fin 2 - Alignment notches cut into the side to match the alignment pins on the graphite fixture

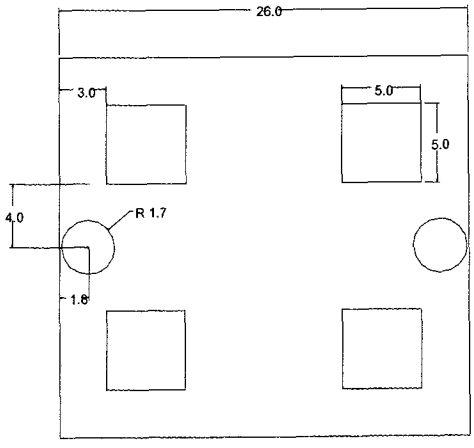

Figure 23: Channel 3 - Final design used. Alignment holes added to match with fixturing device

APPENDIX E: SCREENING EXPERIMENT DATA

Experiment explanation

The experiment was a 2^2 factorial experiment with material and alignment being the factors.

Each test article was given a different code as follows:

- XXX indicates Ni
  - 400 series indicates poor alignment
  - 500 series indicates good alignment
- XXXX indicates NiAl
  - 4000 series indicates poor alignment
  - 5000 series indicates good alignment

Each test article had two microchannel arrays. These are

- XX0 indicates first array
- XX1 indicates second array

Each microchannel array had 3 channels designated:

- XXX-A designates top channel
- XXX-B designates middle channel
- XXX-C designates bottom channel

NiAl Data

Sample #	Alignment	Mag	inside channel Measured hannel (mr	Mag	end channel Measured End (mm)	inside channel Adjusted Channel	end channel Adjusted End	inside channel Channel Avg	inside channel Std. Dev.	end channel End Avg.	end channel Std. Dev
5001-A	Poor	25	7	27	4.5	0.28	0.17	0.27	0.050332	0.19	0.021383
		25	8	27	5.5	0.32	0.20				
		25	5.5	27	5.5	0.22	0.20				
5001-B	Poor	25	5	27	7	0.20	0.26	0.21	0.011547	0.31	0.048995
		25	5.5	27	9.5	0.22	0.35				
		25	5	27	9	0.20	0.33				
5001-C	Poor	25	6	27	6	0.24	0.22	0.21	0.030551	0.19	0.028288
		25	5	27	5	0.20	0.19				
		25	4.5	27	4.5	0.18	0.17				
5000-A	Poor	27	5	34	4	0.19	0.12	0.15	0.038549	0.14	0.033962
		27	4.5	34	4	0.17	0.12				
		27	3	34	6	0.11	0.18				
5000-B	Poor	27	4	34	9	0.15	0.26	0.19	0.037037	0.24	0.029412
		27	6	34	7	0.22	0.21				
		27	5	34	8	0.19	0.24				
5000-C	Poor	27	4	34	3	0.15	0.09	0.19	0.037037	0.14	0.044927
		27	5	34	6	0.19	0.18				
		27	6	34	5	0.22	0.15				
4001-A	Good	28	3	29	4	0.11	0.14	0.11	0.01031	0.14	0
		28	3	29	4	0.11	0.14				
		28	3.5	29	4	0.13	0.14				
4001-B	Good	28	4	29	4.5	0.14	0.16	0.17	0.02062	0.16	0.009954
		28	5	29	5	0.18	0.17				
		28	5	29	4.5	0.18	0.16				
4001-C	Good	28	4.5	29	1.5	0.16	0.05	0.14	0.030929	0.08	0.08148
		28	4.5	29	0.5	0.16	0.02				
		28	3	29	5	0.11	0.17				
4000-A	Good	27	1.5	32	4	0.06	0.13	0.07	0.021383	0.11	0.015625
		27	1.5	32	3	0.06	0.09				
		27	2.5	32	3.5	0.09	0.11				
4000-B	Good	27	3.5	32	4	0.13	0.13	0.14	0.010692	0.12	0.009021
		27	4	32	4	0.15	0.13				
		27	3.5	32	3.5	0.13	0.11				
4000-C	Good	27	3	32	6	0.11	0.19	0.12	0.021383	0.16	0.03125
		27	3	32	5	0.11	0.16				
		27	4	32	4	0.15	0.13				

Ni Data

Sample #	Alignment	inside channel Mag	inside channel Measured Channel (mm)	end channel Mag	end channel Measured End (mm)	inside channel Adjusted Channel	end channel Adjusted End	inside channel Channel Avg	inside channel Std. Dev.	end channel End Avg.	end channel Std. Dev
401-A	Poor	28	4.5	29	5	0.16	0.17	0.17	0.01031	0.17	0
		28	4.5	29	5	0.16	0.17				
		28	5	29	5	0.18	0.17				
401-B	Poor	28	5.5	29	5	0.20	0.17	0.20	0.017857	0.16	0.009954
		28	6	29	4.5	0.21	0.16				
		28	5	29	4.5	0.18	0.16				
401-C	Poor	28	5.5	29	5	0.20	0.17	0.18	0.01031	0.17	0
		28	5	29	5	0.18	0.17				
		28	5	29	5	0.18	0.17				
400-A	Poor	28	4.5	29	5	0.16	0.17	0.17	0.01031	0.17	0
		28	4.5	29	5	0.16	0.17				
		28	5	29	5	0.18	0.17				
400-B	Poor	28	5	29	4.5	0.18	0.16	0.17	0.01031	0.16	0
		28	4.5	29	4.5	0.16	0.16				
		28	5	29	4.5	0.18	0.16				
400-C	Poor	28	3.5	29	4.5	0.13	0.16	0.11	0.01031	0.14	0.009954
		28	3	29	4	0.11	0.14				
		28	3	29	4	0.11	0.14				
300-A	Good	27	4	29	5	0.15	0.17	0.14	0.021383	0.17	0.009954
		27	3	29	4.5	0.11	0.16				
		27	4	29	5	0.15	0.17				
300-B	Good	27	3.5	29	4	0.13	0.14	0.15	0.018519	0.16	0.017241
		27	4	29	4.5	0.15	0.16				
		27	4.5	29	5	0.17	0.17				
300-C	Good	27	5	29	4	0.19	0.14	0.22	0.038549	0.16	0.019909
		27	7	29	5	0.26	0.17				
		27	5.5	29	5	0.20	0.17				
301-A	Good	28	4	27	4.5	0.14	0.17	0.13	0.017857	0.17	0.010692
		28	3	27	5	0.11	0.19				
		28	3.5	27	4.5	0.13	0.17				
301-B	Good	28	5	27	4	0.18	0.15	0.18	0.01031	0.13	0.018519
		28	5	27	3	0.18	0.11				
		28	5.5	27	3.5	0.20	0.13				
301-C	Good	28	4	27	5	0.14	0.19	0.14	0.01031	0.19	0
		28	4	27	5	0.14	0.19				
		28	3.5	27	5	0.13	0.19				

Sum of Squares calculations

	AVG/SD PER CHANNEL	Ni mean	Ni SD	NiAl mean	NiAl SD
		0.17	0	0.19	0.021383
		0.16	0.00995	0.31	0.048995
Poor		0.17	0	0.19	0.028288
Alignment		0.17	0	0.14	0.033962
		0.16	0	0.24	0.029412
		0.14	0.0095	0.14	0.044927
	Avg	0.161667	0.003242	0.201667	0.034495
	SOS	0.002109	0.000141	0.002109	0.000141
		0.17	0.00995	0.14	0
		0.16	0.01724	0.16	0.009954
Good		0.16	0.01991	0.08	0.08148
Alignment		0.17	0.01069	0.11	0.015625
		0.13	0.01852	0.12	0.009021
		0.19	0	0.16	0.03125
	Avg	0.163333	0.012718	0.128333	0.024555
	SOS	0.002109	0.000141	0.002109	0.000141

Poor Alignment Grand Avergages

Width	0.181667 SOS	0.003852
STD%	0.018868 SOS	1.61E-07

Sch 0.007704 Width sum of squares for channel alignment
3.21E-07 STD%

Good Alignment Grand Avergages

Width	0.145833 SOS	0.003852
STD%	0.018637 SOS	1.61E-07

	Ni Grand Avg	Ni Grand SOS	NiAl Grand Avg	NiAl Grand SOS
Width	0.1625	1.88E-05	0.165	1.87E-05
STD%	0.00798	0.001393	0.029525	0.001393

Overall Averages

Width	0.16375
STD%	0.018752

Sm 3.75E-05 Width sum of squares for material
0.002785 STD%

SI 0.008437 sum of squares for factor interaction
0.000565

Ni avg	Ni sd	NiAl avg	NiAl sd	avg	sd	avg	sd
0.17	0	0.19	0.021383	6.944E-05	1.05E-05	0.000136	0.000172
0.16	0.00995	0.31	0.048995	2.778E-06	4.5E-05	0.011736	0.00021
0.17	0	0.19	0.028288	6.944E-05	1.05E-05	0.000136	3.85E-05
0.17	0	0.14	0.033962	6.944E-05	1.05E-05	0.003803	2.84E-07
0.16	0	0.24	0.029412	2.778E-06	1.05E-05	0.001469	2.58E-05
0.14	0.0095	0.14	0.044927	0.0004694	3.92E-05	0.003803	0.000109
0.161667	0.003242	0.201667	0.034495				
0.17	0.00995	0.14	0	4.444E-05	7.66E-06	0.000136	0.000603
0.16	0.01724	0.16	0.009954	1.111E-05	2.04E-05	0.001003	0.000213
0.16	0.01991	0.08	0.08148	1.111E-05	5.17E-05	0.002336	0.00324
0.17	0.01069	0.11	0.015625	4.444E-05	4.11E-06	0.000336	7.97E-05
0.13	0.01852	0.12	0.009021	0.0011111	3.37E-05	6.94E-05	0.000241
0.19	0	0.16	0.03125	0.0007111	0.000162	0.001003	4.48E-05
0.163333	0.012718	0.128333	0.024555				

Se(Avg) Se(SD) sum of squares for error
0.028583 0.005384

3.91E-05	0.000352	0.000689	6.92E-06
1.41E-05	7.75E-05	0.021389	0.000915
3.91E-05	0.000352	0.000689	9.09E-05
3.91E-05	0.000352	0.000564	0.000231
1.41E-05	0.000352	0.005814	0.000114
0.000564	8.56E-05	0.000564	0.000685
3.91E-05	7.75E-05	0.000564	0.000352
1.41E-05	2.29E-06	1.41E-05	7.74E-05
1.41E-05	1.34E-06	0.007014	0.003935
3.91E-05	6.5E-05	0.002889	9.78E-06
0.001139	5.4E-08	0.001914	9.47E-05
0.000689	0.000352	1.41E-05	0.000156

0.16375 Ovl Avg Overall average channel width
0.0187524 Ovl SD Overall channel width deviation

0.044763 Stotal (avg) total sum of squares
0.008735 Stotal (SD)